Enhanced Magnetism in Highly Ordered Magnetite Nanoparticle-Filled Nanohole Arrays

Binh Duong, Hafsa Khurshid, Palash Gangopadhyay, Jagannath Devkota, Kristen Stojak, Hariharan Srikanth, Laurene Tetard, Robert A. Norwood, N. Peyghambarian, Manh-Huong Phan, and Jayan Thomas**

***A** new approach to develop highly ordered magnetite (Fe_3O_4) nanoparticle-patterned nanohole arrays with desirable magnetic properties for a variety of technological applications is presented. In this work, the sub-100 nm nanohole arrays are successfully fabricated from a pre-ceramic polymer mold using spin-on nanoprinting (SNAP). These nanoholes are then filled with monodispersed, spherical Fe_3O_4 nanoparticles of about 10 nm diameter using a novel magnetic drag and drop procedure. The nanohole arrays filled with magnetic nanoparticles are imaged using magnetic force microscopy (MFM). Magnetometry and MFM measurements reveal room temperature ferromagnetism in the Fe_3O_4-filled nanohole arrays, while the as-synthesized Fe_3O_4 nanoparticles exhibit superparamagnetic behavior. As revealed by MFM measurements, the enhanced magnetism in the Fe_3O_4-filled nanohole arrays originates mainly from the enhanced magnetic dipole interactions of Fe_3O_4 nanoparticles within the nanoholes and between adjacent nanoholes. Nanoparticle filled nanohole arrays can be highly beneficial in magnetic data storage and other applications such as microwave devices and biosensor arrays that require tunable and anisotropic magnetic properties.*

1. Introduction

Nanoarchitecturing of thin films has emerged as a straightforward and effective way to engineer materials' properties at the nanometer level. Currently, there is an increasing need for the use of nanostructured materials with tunable and anisotropic magnetic properties.[1] However, the ability to tune the magnetic anisotropy of magnetic nanoparticles to meet the needs of vastly different applications is a challenge. While magnetite (Fe_3O_4) nanoparticles are widely used in magnetic resonance imaging (MRI) and biomedical applications,[2] they have recently been incorporated into a polymer matrix to create a new class of lightweight nanocomposite materials with enhanced and tunable microwave properties.[3] The use of such nanoparticles provides a route to a low-cost microwave substrate. This technology thus offers a new approach for fabrication of high-performance RF and microwave devices, such as integrated high-Q inductors and filters.[3,4] However, the dispersion of magnetic nanoparticles into a

Dr. B. Duong,[+] L. Tetard, Prof. J. Thomas
NanoScience Technology Center
University of Central Florida
FL 32826, USA
E-mail: Laurene.Tetard@ucf.edu;
Jayan.Thomas@ucf.edu

Dr. H. Khurshid,[+] J. Devkota, K. Stojak, Prof. H. Srikanth, Prof. M.-H. Phan
Department of Physics
University of South Florida
FL 33620, USA
E-mail: phanm@usf.edu

Dr. P. Gangopadhyay,[+] Prof. R. A. Norwood, Prof. N. Peyghambarian
College of Optical Sciences
University of Arizona
AZ 85721, USA

[+]B. D., H. K. and P. G. contributed equally to this work.

DOI: 10.1002/smll.201303809

polymer matrix is a challenging task for the fabrication of this kind of nanocomposite, since a simple blending of particles and polymer can result in aggregation of particles. As a matter of this fact, further enhancement in the magnetic and microwave responses in such nanocomposites is not feasible by simply loading more particles into the polymer matrix. The tunability of the magnetic anisotropy is also hardly achievable in this nanostructure, since magnetic nanoparticles are randomly distributed throughout the polymer matrix. Recently, Qin et al. have reported on a new class of microwave composites, which is composed of high-aspect ratio magnetic microwires embedded into a polymer matrix.[1a,5] The authors have shown that the microwave properties of the composite can be enhanced by tuning the saturation magnetization and magnetic anisotropy of microwires. However, the fabrication technique developed does not enable the creation of nanocomposite materials with highly ordered wire arrays and small wire spacing (limited to 3 mm wire spacing).[5] To overcome these challenging issues, it is essential to develop a technique that allows the creation of highly ordered magnetic nanoparticle-filled nanohole arrays in a polymer film. Furthermore, there has been growing interest in developing highly ordered magnetic nanostructures for applications like high density magnetic storage media.[6] The push to increase data density and the rate of data recording has been the driving force behind recent advancements in magnetic recording media. One of the most challenging tasks is to maintain sufficiently high magnetic anisotropy of the particles, in order to stabilize recorded information, in these media while simultaneously reducing their particle sizes to increase information storage density. In this case, it is crucial to understand how magnetic dipole interactions of particles within nanoholes and between adjacent nanoholes affect the magnetism of the medium.

In an effort to realize such magnetic effects at the nanoscale, it is critical to have approaches that offer versatile fabrication capabilities. Nevertheless, the success of such fabrication depends not only on nanofabrication techniques, but also on approaches that offer low-cost operation and high throughput, suitable for mass production. So far, most of the published works rely on lithography-based processes such as photolithography,[7] focused-ion beam lithography,[8] and deep-UV lithography.[9] The disadvantages of these approaches include long processing time, complicated procedures, high cost, and limited scalability. Alternatively, bottom-up approaches such as self-assembly[10] have been utilized as well. However, these methods are only viable in selected materials and it is difficult to control pattern dimensions. Another technique to fabricate nanostructures is by using anodic aluminum oxide (AAO)[11] templates to grow or deposit desirable materials. The AAO templates are not chemically stable over long periods of time, so they eventually need to be removed, a process which adversely affects the properties of the final nanostructures. To overcome these drawbacks, several unconventional lithographic techniques have been developed including nanoimprint lithography (NIL),[12] microcontact printing,[13] and replica molding.[14] The feature size produced by these techniques is currently restricted by the size of the master mold, which needs to be separately fabricated by electron beam lithography. To study any phenomena at a smaller size, it is necessary to create a new silicon mold, which is not practical for many applications. Additionally, Si molds often require surface modifications after several printings in order to maintain structural integrity during the demolding process. Realizing this void in the current technology, we recently developed a facile nanoarchitecturing technique called SNAP, to fabricate pre-ceramic polymer structures (2nd generation) from a master mold (1st generation).[15,16] The printed patterns can be effectively used as a mold for printing 3rd generation patterns; hence, inverted patterns with a smaller feature size can be obtained without fabricating a new silicon master mold. Moreover, it is also possible to plasma etch the second generation structures to tune the size of the third generation nanostructures. The complete fabrication process of the 2nd and 3rd generation patterns (1cm × 1cm area) can be achieved in less than 10 minutes using commonly available and inexpensive lab equipment such as a spin coater and hot plate. If these nanohole arrays can be filled with magnetic particles to create a new class of novel high-aspect ratio magnetic nanocomposites, the challenges raised above can be resolved. With this motivation, we present a simple and high throughput method to develop an array of Fe_3O_4 nanoparticle-filled nanoholes and demonstrate the unique magnetic properties of the material for a variety of applications.

2. Arrays of Nanoholes Filled Fe_3O_4 Nanoparticles and Magnetic Properties

2.1. Process of Filling Nanoholes with Magnetite Nanoparticles

A schematic of the novel process we developed to fill large area arrays of nanoholes with Fe_3O_4 nanoparticles is shown in **Figure 1**. This process was accomplished in three steps: (1) fabricating a pre-ceramic mold, (2) forming the required nanohole patterns on polyacrylinitrile (PAN) film and (3) trapping the Fe_3O_4 nanoparticles within the nanosized holes. Details on preparation of the mold have been described in Ref.[15].

A magnetic drag and drop method was established to fill the nanoholes with Fe_3O_4 particles. As the first step, a dispersion of 10 nm Fe_3O_4 nanoparticles was drop-casted on to the patterned film. After solvent evaporation, Fe_3O_4 nanoparticles still remained on the surface of the film. Since single domain Fe_3O_4 particles are uniformly magnetized at room temperature, we guided the nanoparticles into the patterned holes by moving a magnet of 0.65 T underneath the substrate in one direction. The stray particles remaining on the surface of the film were removed by dragging them out of the nanohole area using the magnet. Washing with excess solvent (hexane) ensured that no particles were left behind on the surface.

Figure 2a shows a bright-field TEM image of the synthesized Fe_3O_4 nanoparticles. The nanoparticles are spherical, with an average diameter of 10.5 ± 0.5 nm determined by fitting the distribution obtained after counting more than 200 particles (Figure 2b). The HRTEM image of the nanoparticles (Figure 2c) evidences that the nanoparticles are single crystalline, as the lattice fringes continue without interruption. The calculated distance between the lattice planes in Figure 2c is 2.1 Å, which corresponds to the (400) planes

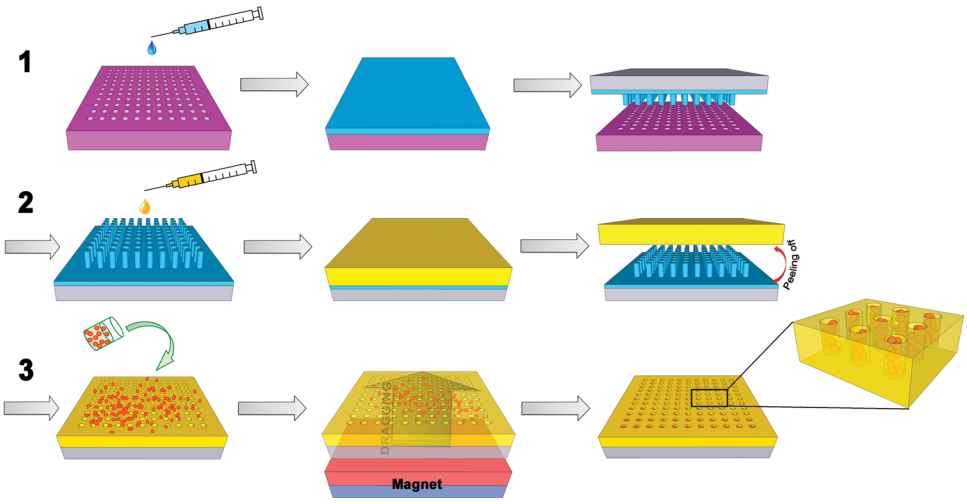

Figure 1. Schematic showing the steps involved in (1) fabricating PUS nanopillar structures from a silicon mold (2) printing of PAN nanoholes patterns from the PUS mold (3) filling of Fe_3O_4 nanoparticles into the nanoholes: a solution of Fe_3O_4 nanoparticles was drop-casted onto the hole arrays; the particles were dragged into the holes by a magnet. Stray particles remaining on the surface were washed away with excess solvent.

of Fe_3O_4. Figure 2d shows the XRD pattern of the nanoparticles. All peaks are indexed to the characteristic reflections of Fe_3O_4 crystal planes. The average crystalline size, as determined from peak widths using the modified Scherrer's formula,[17] is about 9 nm. This size is very close to that determined from the TEM, confirming the single crystalline nature of the synthesized particles. Figure 2e shows a selected area electron diffraction (SAED) image of the nanoparticles. All diffraction rings correspond to those of Fe_3O_4, which is consistent with the measured XRD pattern.

Figure 3a and b show SEM images of the printed nanohole arrays before and after filling with the magnetite particles. As shown in Figure 3c, uniform distribution of Fe_3O_4 nanoparticles still reside in the nanoholes after washing and removing stray particles on the patterned surface. It should be noted that the grainy texture on the ridges (Figure 3a and c) is the result of the platinum coating, which was used as the conductive layer for SEM imaging. To examine the diameter and depth of the nanoholes, we studied the SEM and AFM images obtained and the average diameter of the nanoholes observed from AFM and SEM were in good agreement. A careful data analysis of the AFM topography images (**Figure 4**) indicated a distribution in diameter that is centered around 95 nm (as indicated in the inset of Figure 4a), while SEM images indicate 80 nm. The variation can be attributed to the tip effect in the AFM measurements. The average depth of these nanoholes is about 90 nm with a center-to-center distance of about 200 nm. However, the depth profiles are limited by the depth perception of the tips (also known as AFM tip artifact), meaning that these depth profiles are most likely less than the actual depth. Note that the penetration of the AFM tip was nonetheless sufficient to resolve nanoparticles in the nanoholes as seen in Figure 4b.

We utilized MFM to confirm that multiple Fe_3O_4 nanoparticles are indeed inside the holes, and to study their effect on the nanoarchitectured thin films. The measurements were performed in tapping (AC) mode, using a permanently magnetized tip (see methods) and a two-pass technique. During the first pass, the tip records the surface topography along a line and registers the trajectory. The tip is then lifted 50 nm above the surface and the same line of the sample is re-scanned, at constant height, following the trajectory acquired during the first pass. Figure 4a shows the topography of the nanoholes (obtained during the first pass) while Figure 4b

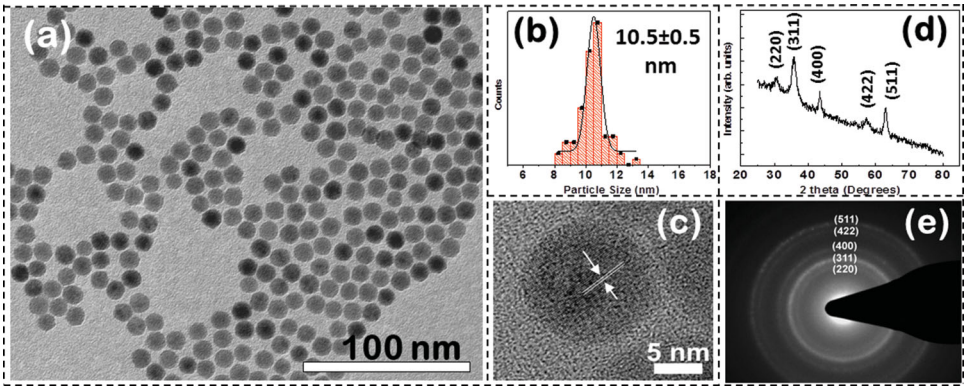

Figure 2. Bright-field TEM image of as-synthesized Fe_3O_4 nanoparticles (a), the corresponding particle size distribution (b), HRTEM image of a single Fe_3O_4 nanoparticle (c), XRD pattern (d) and SAED image of the Fe_3O_4 nanoparticles (e).

NANO MICRO small

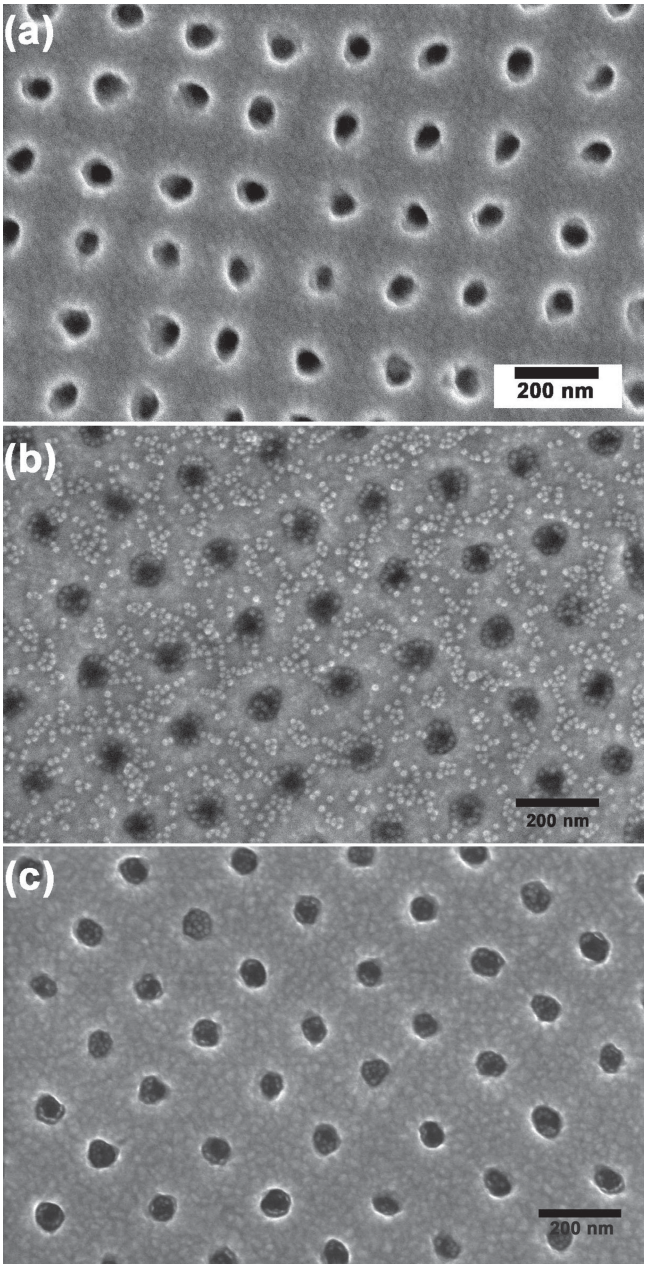

Figure 3. SEM images show arrays of nanoholes (a) before and (b) after filled with Fe_3O_4 nanoparticles and (c) after removing stray particles.

constitutes the MFM map (phase image recorded in the second pass). During the second pass the cantilever is lifted 50 nm above the surface to limit the contribution of short-range forces in the MFM image. During the magnetic measurement, the feedback loop varies with the attractive or repulsive nature of the localized tip-sample magnetic forces. The phase of the signal is acquired to form the images of the magnetic force gradient presented here. A darker color (i.e. red to black) in the MFM image (Figure 4b) indicates an attractive magnetic interaction between the sample, superparamagnetic nanoparticles and the magnetized tip, which can also be understood as a variation in the out of plane magnetic poles. Considering the out of plane direction of the field imposed by the magnetic tip, the results provide a first indication of the nanoparticles' properties in the nanoholes, as the pattern of dark regions in the film clearly matches the location of the nanoparticle-filled-holes. The detected magnetic response of the nanoholes can be attributed to the collective nature of magnetic forces originating from the cumulative stray field of closely packed individual particles.

The insets in Figure 4b provide another indication of the response of the nanoholes across the samples with a full width at half maximum (FWHM) around 19 nm while the roundness (i.e. how well the shape considered matches with a perfect disc (roundness = 1.0)) was centered at 0.90 in the MFM measurements (bottom inset Figure 4b).

2.2. Magnetic Properties of Fe_3O_4 Nanoparticles and Fe_3O_4-Filled Nanoholes

It is generally accepted that the practical applications of magnetic nanowire arrays require a deep understanding of the magnetism of nanowires.[18–20] Therefore, in the present work, we performed a comparative study of the magnetic properties of as-synthesized Fe_3O_4 nanoparticles with the Fe_3O_4-filled nanohole film. **Figure 5** displays the temperature dependence of the zero-field-cooled (ZFC) and field-cooled (FC) magnetization (M–T) taken at a field of 50 mT for the Fe_3O_4 nanoparticles (a) and for the Fe_3O_4-filled nanohole film (b). The inset of Figure 5a shows the M–T curves taken at a field of 10 mT for the Fe_3O_4 nanoparticles. In a ZFC measurement protocol, the sample was cooled from 300 K to 5 K without applying a magnetic field. After reaching 5 K, a field of 50 mT was applied and the magnetization was measured as a function of temperature upon heating up to 300 K. For a FC measurement, the sample was cooled from 300 K to 5 K in the presence of a field of 50 mT and the magnetization was recorded upon increasing the temperature.

As can be seen in Figure 5a and its inset, the Fe_3O_4 nanoparticle sample shows a transition from the ferromagnetic (blocked) state to the superparamagnetic state with increasing temperature. This transition temperature, corresponding to the maximum in the ZFC M–T curve, is often referred to as the mean blocking temperature (T_B), which is proportional to the effective anisotropy constant (K_u) and magnetic volume (V) of the particle via $T_B = K_u V/25k_B$, where k_B is the Boltzmann constant. Using this relationship, the K_u of the 10 nm Fe_3O_4 particles is evaluated to be $\approx 8.24 \times 10^4$ J/m^3, which is slightly larger than that of bulk Fe_3O_4 (1.35×10^4 J/m^3). This enhancement of the particle anisotropy is likely associated with the dipolar interactions, rather than a surface with larger anisotropy.[28] The temperature below which the ZFC and FC M–T curves begin to separate from each other is referred to as the irreversibility temperature (T_{irr}), which is associated with the blocking of the biggest particles. It has been noted that a particle system with T_{irr} well above T_B often shows a large particle size distribution.[21] The proximity between the T_B and T_{irr} values is a signature of the monodisperse nature of our Fe_3O_4 nanoparticles and clearly excludes the presence of a large extent of particle aggregation or a large size distribution, which is consistent with the TEM images (10.5 ± 0.5 nm). As a result, the

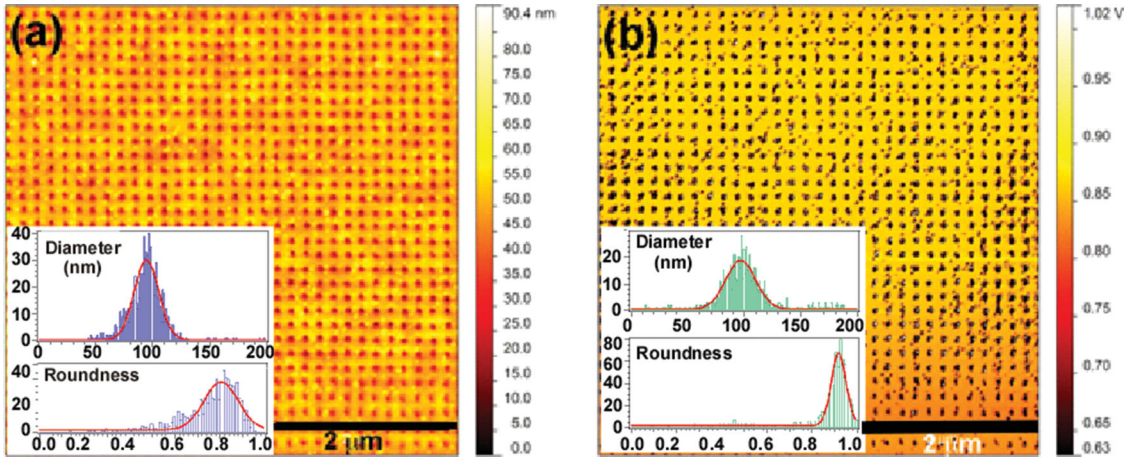

Figure 4. (a) AFM topography image of a nano-patterned array of holes filled with 10 nm Fe_3O_4 nanoparticles; (b) MFM image of the same region. The size distribution of the nanoholes as extracted from AFM topography image of a nano-patterned array of holes (top inset in a) and MFM image of the nano-patterned array of holes filled with 10nm Fe_3O_4 nanoparticles (top inset in b). Roundness distribution of the nanoholes signals as extracted from AFM topography image of a nano-patterned array of holes (bottom inset in a) and MFM image of the nano-patterned array of holes filled with 10nm Fe_3O_4 nanoparticles (bottom inset in b).

broadening of the ZFC M–T curve observed for the Fe_3O_4 nanoparticles (inset of Figure 5a) is not attributed to a large particle size distribution, but results from the weak dipolar inter-particle interactions that are present in the sample. It is also noted that as the applied magnetic field was increased from 10 mT (inset of Figure 5a) to 50 mT (Figure 5a), the T_B decreased from 125 K to 116 K, respectively. This magnetic field dependence of T_B can be related to the fact that a magnetic field lowers the energy barriers between the two easy axis orientations and thus the T_B.[22]

The case is quite different for the Fe_3O_4-filled nanohole film (Figure 5b). The ZFC M–T curve shows a sharp peak around 77 K, with a strong increase in the FC magnetization with temperature below ≈150 K. The T_{irr} appears at ≈125 K, below which a large separation between the ZFC and FC magnetization is observed. Above 150 K, both the ZFC and FC magnetization coincide and decrease gradually with increasing temperature. The reason for this difference may be due to the additional magnetic dipole interactions between the large effective moments of the filled nanoholes and magnetic texture formed in nanoholes due to strong shape anisotropy, as well as enhanced surface spin disorder. These factors have been reported to have a strong impact on the magnetism of magnetic nanowire arrays.[18–20,23]

To further elucidate these intriguing features, we measured the magnetic hysteresis (M-H) loops at 300 K and 10 K for both the as-synthesized Fe_3O_4 nanoparticles and the Fe_3O_4-filled nanohole film. The results are shown in **Figure 6**. As one can see in Figure 6a and c, for the as-synthesized Fe_3O_4 nanoparticles, the M-H curves at 300 K do not show any hysteresis (zero coercivity, H_C, and no remnant magnetization, M_r), whereas a clear hysteresis with a coercivity of $H_C \approx 53$ mT is observed at 10 K. This is characteristic of the sample of nanoparticles being superparamagnetic at room temperature and entering a ferromagnetic (blocked) state at low temperature, which results in the opening up of the hysteresis loop. This finding is in agreement with the M–T curves (Figure 5a). However, the case is very different for the Fe_3O_4-filled nanohole film (Figure 6b and d). The M-H curve of this sample at 300 K shows a clear hysteresis, with values of $H_C \approx 30$ mT and $M_r/M_S \approx 0.2$ as displayed in the inset of Figure 6b. This feature is rather different from that observed previously by us for the case of carbon nanotubes (CNTs) filled with Fe_3O_4 nanoparticles, where filling CNTs with Fe_3O_4

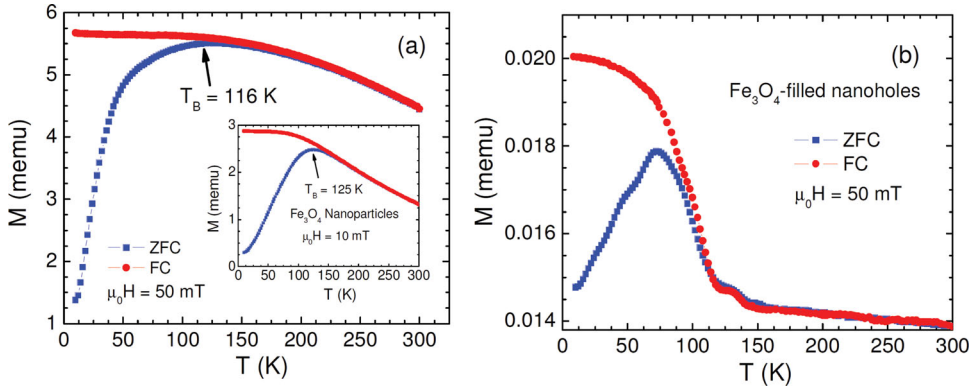

Figure 5. Temperature dependence of ZFC and FC magnetization (M–T) taken at a field of 50 mT for the Fe_3O_4 nanoparticles (a) and for the Fe_3O_4-filled nanohole film (b). The inset of Figure 5a shows the M–T dependence for an external magnetic field of 10 mT for the Fe_3O_4 nanoparticles.

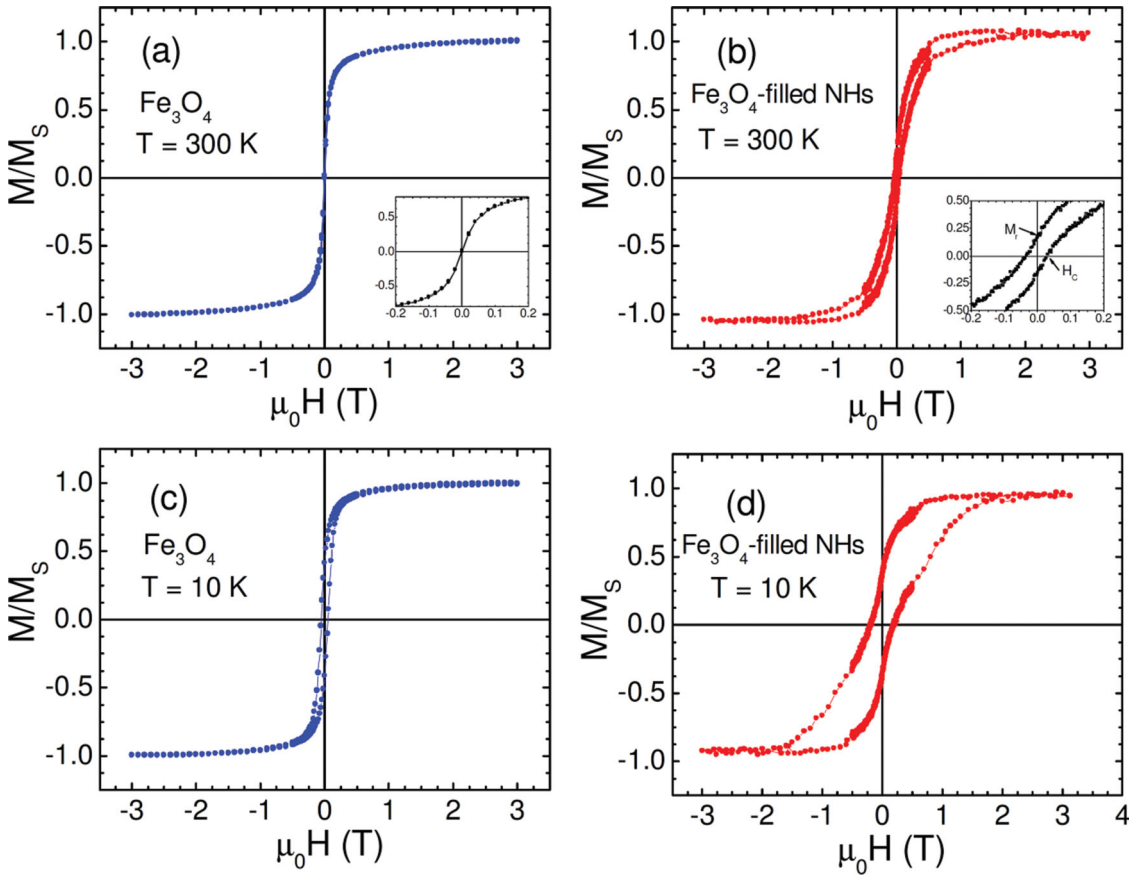

Figure 6. Magnetic hysteresis (M-H) loops taken at 300 K and 10 K for the as-synthesized Fe_3O_4 nanoparticles (a, c) and for the Fe_3O_4-filled nanohole film (b, d). The insets of Figure 6a and b show the enlarged low-field M-H curves.

nanoparticles was found to preserve the superparamagnetic nature of the nanoparticles at room temperature.[24] In the latter case, the enhancement of dipolar inter-particle interactions was shown to result in larger values of T_B and H_C for the Fe_3O_4-filled CNTs relative to the Fe_3O_4 nanoparticles. It was reported that at 5 K the coercive field of the Fe_3O_4-filled CNTs ($H_C \approx 13$ mT) was about 3 times larger than that of the Fe_3O_4 nanoparticles ($H_C \approx 4.5$ mT). However, in the present case the coercive field of the Fe_3O_4-filled nanohole film ($H_C \approx 216$ mT) measured at 10 K is more than 4 times that of the Fe_3O_4 nanoparticles ($H_C \approx 51$ mT). These results suggest that other factors in addition to enhanced inter-particle interactions are also important in governing the magnetism of the Fe_3O_4-filled nanohole film.

To quantitatively interpret the origin of the enhanced H_C in the Fe_3O_4-filled nanohole film, we considered the relative contributions to the coercivity from the shape anisotropy energy of quasi-1D nanoholes and the magnetocrystalline anisotropy energy of the nanoparticles. It has been reported that in the case of an array of magnetic nanowires, the coercivity can be evaluated as

$$H_C = \frac{4\,L_{ex}^2 q^2 M_S}{D^2} + P_C \frac{K_1^2}{M_S A} d^2 \qquad (1)$$

where the first term is related to the contribution of the shape anisotropy energy of nanowires and the second term results from the contribution of the magnetocrystalline anisotropy energy of nanoparticles.[25] M_S is the saturation magnetization, D is the average diameter of a nanowire, d is the particle diameter, K_1 is the first-order magnetic anisotropy constant, A is the exchange stiffness constant, P_C is a coefficient, $L_{ex} = (A/K_1)^{1/2}$ is the magnetic exchange length, and q is the smallest solution of the Bessel functions. Using Equation (1) with $M_S = 2.91 \times 10^4$ A/m and $K_1 \cong K_u/12 = 0.68 \times 10^4$ J/m^3 for our Fe_3O_4 nanoparticles, $q = 1.84$, $A = 10^{-11}$ J/m, $P_C = 0.5$, $L_{ex} = 38.3$ nm, $d = 10$ nm, and $D = 80$ nm, the H_C of the Fe_3O_4-filled nanohole film is estimated to be ≈124 mT. This value is significantly smaller than that obtained experimentally ($H_C \approx 216$ mT). Since Equation (1) does not take into account the magnetic dipole interactions between the filled nanoholes, magnetic texture formed in nanoholes due to strong shape anisotropy, and surface spin disorder, the remarkable deviation between the calculated and experimental values of H_C points to the fact that, in addition to the dipolar inter-particle interactions, these effects also contribute significantly to the enhanced H_C. The enhancement in H_C for the case of the Fe_3O_4-filled nanohole film is in excellent agreement with that in the effective magnetic anisotropy field (H_K). Here, H_K is estimated as the maximum in the dM/dH vs. H curves (dM/dH is the derivative of magnetization with respect to magnetic field), from the M-H data. We have found that the H_K values of the Fe_3O_4-filled nanohole film at 300 K (H_K = 4.97 kOe) and 10 K (H_K = 12.219 kOe) are ≈3 and ≈6 times

larger than those of the powder Fe_3O_4 particles (H_K = 1.36 kOe and 2.14 kOe for 300 K and 10 K, respectively). Unlike the case of the as-synthesized Fe_3O_4 nanoparticles, a kink appeared in the low-field M-H loops for the Fe_3O_4-filled nanohole film (Figure 6b and d). This can be attributed to the competition between the demagnetization energy of quasi-1D nanostructure and the magnetocrystalline anisotropy energy of nanoparticles in nanoholes. A similar phenomenon has also been reported for $La_{0.7}Sr_{0.3}MnO_3$ films composed of magnetic nanocolumnar structures.[26]

2.3. Magnetic Force Microscopy Characterization of Nanoholes Filled with Fe_3O_4 Nanoparticles

To gain deeper insights into the nature of the magnetic properties of Fe_3O_4 nanoparticles within the nanoholes, as well as between the adjacent nanoholes, MFM profiling was performed on the region of the Fe_3O_4-filled nanohole film as presented in **Figure 7**. In our MFM measurements, the constant magnetization of the tip and its oscillation above the sample constitute a force gradient directed perpendicular to the plane of the film. The contrast seen in the MFM image (Figure 7a) can be attributed to an out-of-plane component of the magnetization, which oscillates in up and down directions to reduce the magnetostatic energy, creating magnetic poles of alternating signs that give rise to the lower and higher phase of the tip oscillation.[27] It has been reported that the presence of vortex domains could give rise to variations in the MFM phase contrast in magnetic nanowire arrays. However, this possibility can be ruled out in the present case, since we used monodispersed single domain superparamagnetic Fe_3O_4 nanoparticles. As one can see in Figure 7a, the MFM pattern evidences the presence of both diametric and in-axis magnetic moments. A signal with higher intensity, shown in white here, from the diametric magnetic moment (white lobes) clearly stands out. To quantify the strength of the magnetic moments, MFM profiles (vertical/horizontal directions) across five holes in Figure 7a were collected. The sharp spike (few nm to 30 nm in width) at the center of the line profiles shows the in-axis magnetic moment (Figure 7b). Note that given the small size of the sharp spike, it is difficult to create a profile crossing the spikes in each hole. MFM profiles collected from the planar region across the white lobes at the center of the square matrix are shown in Figure 7c. The strength of the in-axis and diametric magnetic moments collected from the four scan diametric lines in the center of Figure 7a is shown in Figure 7d. It is worth noting that the strength of the magnetic moments is stronger for the "vertical" case (Figure 7b) than for the "diagonal" case (Figure 7d). This can be attributed to the nanohole-nanohole interactions that appear to be stronger at shorter distances between the Fe_3O_4-filled nanoholes in the former case. Another interesting behavior observed in Figure 4b and Figure 7a is the presence of a bright spot in several nanoholes, with diameters in the range of 2–10 nm. The preliminary evidence suggests that a change of signal induced by single nanoparticles (10 nm) inside nanohole. The effect of the number of nanoparticles present in the nanohole and their organization within the hole (number of layers, defects, etc.) will be the subject of further studies. These findings point to a significant impact of long-range dipolar magnetic interactions between the Fe_3O_4-filled nanoholes on the magnetism of the Fe_3O_4-filled nanohole array, and provide an important understanding of the origin of the enhanced coercivity, as well as the room temperature ferromagnetic-like behavior observed in this novel magnetic nanostructure.

From a magnetic devices application perspective, the enhancements in H_C and H_K achieved in the highly ordered Fe_3O_4 nanoparticle-filled nanohole arrays are desirable for their use as the magnetic media in high-density magnetic recording applications. A large enhancement of the

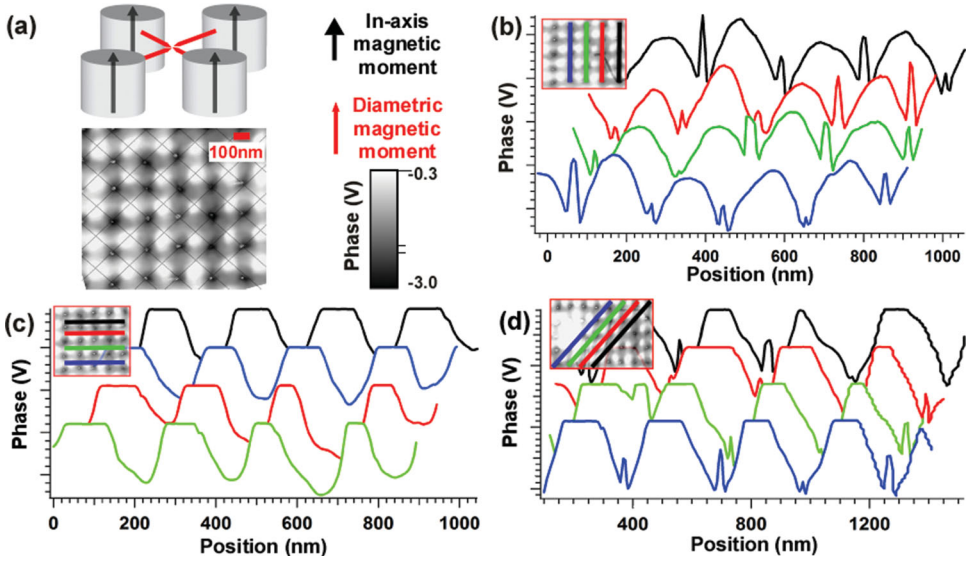

Figure 7. (a) MFM map of about 1μm × 1μm area of the sample with nanoholes filled with Fe_3O_4 nanoparticles. The corresponding magnetic moments of interest are depicted in the inset (top: red arrow for the diametric magnetic moment, black arrow for the in-axis magnetic moment). (b-d) Profiles extracted from the MFM image (a): (b) vertically across the nanoholes, (c) horizontally across the white lobes and (d) diagonally across the nanoholes. The locations are depicted in the respective insets (color coded black, red, green, blue).

microwave response is also expected in these highly ordered Fe_3O_4 nanoparticle-filled nanohole arrays; the coercivity and magnetic anisotropy can easily be tuned by varying the size and density of magnetic nanoparticles inside the nanoholes. This makes the present nanocomposite an attractive candidate for high-performance RF sensor and microwave device applications. Recently, the magnetic anisotropy of Fe_3O_4 nanoparticles has also been exploited to improve the detection capacity of single nanoparticles using the MFM technique.[28] In this regard, the use of a highly ordered Fe_3O_4 nanoparticle-filled nanohole array with tunable magnetic anisotropy seems more favorable for biodetection, as each Fe_3O_4 nanoparticle-filled hole can act as a sensing probe and hence detection of multiple different biomarkers/biomolecules can be achieved simultaneously using this array of patterned multi-holes.

3. Conclusion

We have successfully fabricated sub-100 nm nanohole arrays from a pre-ceramic polymer mold using SNAP lithography. These nano-patterns were uniformly filled with monodispersed 10 nm Fe_3O_4 nanoparticles using a magnetic drag and drop procedure. Magnetization and MFM measurements evidence the enhanced magnetism in the Fe_3O_4-filled nanohole arrays, resulting mainly from the magnetic dipole interactions of Fe_3O_4 nanoparticles within the nanoholes and between adjacent nanoholes. We believe that the simplicity, low cost, short processing time and minimal special equipment requirements of our technique make it favorable for developing novel magnetic nanostructures for applications ranging from high-density magnetic recording and microwave devices to bioengineering.

4. Experimental Section

Synthesis of Fe_3O_4 Nanoparticles: Magnetite (Fe_3O_4) nanoparticles were synthesized using the well-established chemical synthesis technique of thermal decomposition of organometallic compounds.[25b,27a,29] Iron (III) acetyleacetonate Fe-$(acac)_3$ was decomposed at high temperature in the presence of oleic acid and oleylamine. In a typical synthesis, 9 mM of each of oleic acid and oleylamine (with a molar ratio of 0.5) were dissolved in 20 ml octadecene at room temperature. This was followed by the addition of 0.9 mMols of Fe-acac and 3.8 mM of 1,2-hexadecanediol and the mixture was heated to 200 °C under a continuous flow of N_2, along with magnetic stirring. The mixture was homogenized for 2 h at 200 °C under N_2 blanket. The temperature was raised subsequently to 300 °C and refluxed for 1 h. The nanoparticles were washed by adding an excess amount of ethanol followed by centrifuging and dispersion in hexane.

Fabrication of Nanohole Arrays: 1 wt% of dicumyl peroxide was added to polyureasilazane (PUS). The mixture was then filtered and degassed before use. The Si mold was wetted with a commercially available anti-adhesion agent. The PUS precursor was then casted onto the mold and cured for about 30 seconds. The printed film was transferred onto a substrate and used for further study. For clarification purposes, we denote printed pre-ceramic structures as PUS mold. To prepare the medium for second printing, 8 wt% of polyacrylonitrile (PAN, M_w 150 000) was prepared in dimethylformamide and heated at 150 °C.[16,27b,30] The PAN solution was spin-coated onto the PUS mold and cured at 150 °C for about 1 minute. The PAN film was peeled off from the mold and transferred onto a substrate and cured at 250 °C.

Characterization: X-ray diffraction (XRD) was performed on Fe_3O_4 nanoparticles dried on a glass slide. An X-ray diffractometer Bruker AXS D8 was used to analyze crystallographic phases present in the synthesized samples. An FEI Morgagni 268 Transmission Electron Microscope (TEM), operating at an accelerating voltage of 60 kV, and a JEOL JEM 3010FX TEM have been used to characterize the nanoparticles' microstructure and size, and to obtain high-resolution TEM (HRTEM) images. TEM samples were made by dropping a dispersed suspension of particles onto a copper grid covered by a carbon film and allowing the solvent to evaporate. The printed patterns of nanoholes were characterized using a Hitachi H-4800 Scanning Electron Microscope (SEM) and a Veeco Atomic Force Microscope (AFM, Veeco Innova). We used Magnetic Force Microscope (MFM, Veeco Innova) to confirm the presence of Fe_3O_4 nanoparticles inside the nanoholes. A high-resolution custom-made MFM tip (MESP-HR, TN-107) from Veeco with ≈10 nm Cobalt coating on a 5μm long conical antimony doped Si tip (k = 1–3 N/m). Magnetic measurements were conducted on both as-synthesized Fe_3O_4 nanoparticles and on Fe_3O_4-filled nanohole film using a commercial Physical Property Measurement System (PPMS) from Quantum Design with a temperature range of 2–350 K and a superconducting magnet with applied fields of up to ±7 T.

Acknowledgements

J.T acknowledges NSF EAGER (ECCS 1247838) funding for the completion of this work. The authors thank Materials Characterization Facility (MCF), University of Central Florida for the nanostructure characterization. P.G., R. A. N. and N. P. acknowledges funding by the Air Force Office of Scientific Research grant # FA9550–13–1–0101, the Office of Naval Research NECom MURI program and NSF CIAN ERC. Research at USF was supported by the Center for Integrated Functional Materials through grant USAMRMC W81XWH-10–2–0101 and by the DOE through Grant No. DE-FG02–07ER46438. M.H.P. acknowledges support from the Florida Cluster for Advanced Smart Sensor Technologies.

[1] a) F. X. Qin, H. X. Peng, N. Pankratov, M. H. Phan, L. V. Panina, M. Ipatov, V. Zhukova, A. Zhukov, J. Gonzalez, *J. Appl. Phys.* **2010**, *108*, 044510; b) R. C. Che, L. M. Peng, X. F. Duan, Q. Chen, X. L. Liang, *Adv. Mater.* **2004**, *16*, 401; c) G. Korneva, H. H. Ye, Y. Gogotsi, D. Halverson, G. Friedman, J. C. Bradley, K. G. Kornev, *Nano Lett.* **2005**, *5*, 879; d) I. Huynen, G. Goglio, D. Vanhoenacker, A. Vander Vorst, *IEEE Microw. Guided Wave Lett.* **1999**, *9*, 401; e) M. Jaafar, D. Navas, A. Asenjo, M. Vazquez, Hernandez-Velez, J. M. Garcia-Martin, *J. Appl. Phys.* **2007**, *101*, 09F513;

f) V. Skumryev, S. Stoyanov, Y. Zhang, G. Hadjipanayis, D. Givord, J. Nogues, *Nature* **2003**, *423*, 850; g) M. Mito, Y. Komorida, H. Deguchi, T. Tajiri, T. Iwamoto, Y. Kitamoto, *J. Appl. Phys.* **2013**, *113*, 044302.
[2] a) J. Devkota, M. T. Trang, K. Stojak, P. T. Ha, H. N. Pham, T. L. Ngo, N. X. Phuc, D. Mukherjee, H. Srikanth, M. H. Phan, *Sens. Actuators, B* **2014**, *190*, 715; b) C. Sun, J. S. H. Lee, M. Q. Zhang, *Adv. Drug Delivery Rev.* **2008**, *60*, 1252.
[3] K. Stojak, S. Pal, H. Srikanth, C. Morales, J. Dewdney, T. Weller, J. Wang, *Nanotechnology* **2011**, *22*, 135602.
[4] C. Morales, J. Dewdney, S. Pal, S. Skidmore, K. Stojak, H. Srikanth, T. Weller, J. Wang, *IEEE Trans. Microwave Theory Technol.* **2011**, *59*, 302.
[5] F. X. Qin, H. X. Peng, *Prog. Mater. Sci.* **2013**, *58*, 183.
[6] B. D. Terris, T. Thomson, *J. Phys. D: Appl. Phys.* **2005**, *38*, R199.
[7] R. P. Cowburn, A. O. Adeyeye, J. A. C. Bland, *Appl. Phys. Lett.* **1997**, *70*, 2309.
[8] M. Kovylina, M. Erekhinsky, R. Morales, J. E. Villegas, I. K. Schuller, A. Labarta, X. Batlle, *Appl. Phys. Lett.* **2009**, *95*, 152507.
[9] H. X. Wang, Y. C. Wu, M. Wang, Y. G. Zhang, G. H. Li, L. D. Zhang, *Nanotechnology* **2006**, *17*, 1651.
[10] A. A. Zhukov, A. V. Goncharov, P. A. J. de Groot, P. N. Bartlett, M. A. Ghanem, *J. Appl. Phys.* **2003**, *93*, 7322.
[11] S. Pal, S. Chandra, M. H. Phan, P. Mukherjee, H. Srikanth, *Nanotechnology* **2009**, *20*, 485604.
[12] S. Y. Chou, P. R. Krauss, P. J. Renstrom, *Appl. Phys. Lett.* **1995**, *67*, 3114.
[13] J. Zaumseil, M. A. Meitl, J. W. P. Hsu, B. R. Acharya, K. W. Baldwin, Y. L. Loo, J. A. Rogers, *Nano Lett.* **2003**, *3*, 1223.
[14] Y. N. Xia, G. M. Whitesides, *Angew. Chem.-Int. Ed.* **1998**, *37*, 551.
[15] B. Duong, P. Gangopadhyay, J. Brent, S. Seraphin, R. O. Loutfy, N. Peyghambarian, J. Thomas, *ACS Appl. Mater. Interfaces* **2013**, *5*, 3894.
[16] Z. Yu, B. Duong, D. Abbitt, J. Thomas, *Adv. Mater.* **2013**, *25*, 3302.
[17] A. L. Patterson, *Phys. Rev.* **1939**, *56*, 978.
[18] H. Zeng, R. Skomski, L. Menon, Y. Liu, S. Bandyopadhyay, D. J. Sellmyer, *Phys. Rev. B* **2002**, *65*, 134426.
[19] M. T. Chang, L. J. Chou, C. H. Hsieh, Y. L. Chueh, Z. L. Wang, Y. Murakami, D. Shindo, *Adv. Mater.* **2007**, *19*, 2290.
[20] J. Wang, Q. W. Chen, C. Zeng, B. Y. Hou, *Adv. Mater.* **2004**, *16*, 137.
[21] a) Q. Song, Z. J. Zhang, *J. Am. Chem. Soc.* **2012**, *134*, 10182; b) M. B. Morales, M. H. Phan, S. Pal, N. A. Frey, H. Srikanth, *J. Appl. Phys.* **2009**, *105*, 07B511.
[22] G. F. Goya, M. P. Morales, *J. Metastable Nanocrystall. Mater.* **2004**, *20–21*, 673.
[23] X. M. Kou, X. Fan, R. K. Dumas, Q. Lu, Y. P. Zhang, H. Zhu, X. K. Zhang, K. Liu, J. Q. Xiao, *Adv. Mater.* **2011**, *23*, 1393.
[24] S. Pal, S. Chandra, M. H. Phan, P. Mukherjee, H. Srikanth, *Nanotechnology* **2009**, *20*, 485604.
[25] a) L. Sun, Y. Hao, C. L. Chien, P. C. Searson, *IBM J. Res. Dev.* **2005**, *49*, 79; b) J. Xie, S. Peng, N. Brower, N. Pourmand, S. X. Wang, S. H. Sun, *Pure Appl. Chem.* **2006**, *78*, 1003.
[26] D. Mukherjee, M. Hordagoda, R. Hyde, N. Bingham, H. Srikanth, S. Witanachchi, P. Mukherjee, *ACS Appl. Mater. Interfaces* **2013**, *5*, 7450.
[27] a) H. Khurshid, S. Chandra, W. Li, M. H. Phan, G. Hadjipanayis, P. Mukherjee, H. Srikanth, *J. Appl. Phys.* **2013**, *113*, 17B508; b) A. A. Khosroabadi, P. Gangopadhyay, B. Duong, J. Thomas, A. K. Sigdel, J. J. Berry, T. Gennett, N. Peyghambarian, R. A. Norwood, *Phys. Status Solidi A* **2013**, *210*, 831.
[28] T. M. Nocera, J. Chen, C. B. Murray, G. Agarwal, *Nanotechnology* **2012**, *23*, 495704.
[29] G. Sharma, P. Jeevanandam, *RSC Adv.* **2013**, *3*, 189.
[30] B. Cocilovo, A. Amooali, A. Lopez-Santiago, J. Favela, S. Islam, B. Duong, P. Gangopadhyay, M. Fallahi, J. E. Pemberton, J. Thomas, R. A. Norwood, *Appl. Opt.* **2013**, *52*, 1025.

Received: December 12, 2013
Published online: April 6, 2014

